Biomass and Bioenergy 197 (2025) 107778

Contents lists available at ScienceDirect

Biomass and Bioenergy

journal homepage: www.elsevier.com/locate/biombioe

The role of biogenic waste composition on pyrolysis: Part I – Char properties

África Navarro, Isabel Fonts *, Joaquín Ruiz, Jesús Ceamanos, Noemí Gil-Lalaguna, María Benita Murillo, Gloria Gea

Thermochemical Processes Group (GPT), Aragon Institute for Engineering Research (I3A), University of Zaragoza, 50018, Zaragoza, Spain

ARTICLE INFO

Keywords:
Cellulose
Lignin
Protein
$CaCO_3$
Manure
Pyrolysis

ABSTRACT

The yield and properties of char derived from the co-digested manure and its main macro-components, including organic (cellulose, lignin, and protein) components and an inorganic component ($CaCO_3$), produced at different pyrolysis temperatures (350, 550, and 750 °C) have been studied. Experimental results obtained from a surrogate co-digested manure were compared with the theoretically calculated values to explore potential interactions between these macro-components. The char properties analyzed included elemental analysis, pH, FTIR, XPS, and specific surface area. The effect of pyrolysis temperature on many properties was similar, regardless of the precursor (macro-component). Increasing pyrolysis temperature led to higher C content (>90 wt% for cellulose char at 750 °C), pH (from (~7 for cellulose at 350 °C to ~13 for co-digested manure), and specific surface area, observing a marked development of ultramicroporosity and microporosity, especially at the highest pyrolysis temperature studied, 750 °C. An exception was observed for the char derived from proteins due to melting during pyrolysis. By far, the solids from the pyrolysis of cellulose and lignin exhibited the most microporosity development ($SS_{DR} \geq 650\ m^2\ g^{-1}$), reaching, at the highest temperature studied, values close to those of physically activated carbons. Pyrolysis of the surrogate co-digested manure revealed the occurrence of Maillard reactions and also showed an interesting interaction involving $CaCO_3$. The $CaCO_3$ thermal decomposition is promoted when it is embedded into the organic matrix, where the CO_2 generated during decomposition favored the Boudouard reaction of C from the organic components. This results in a lower biochar yield, 32 wt% versus 37 wt % (expected value), and a higher development of microporosity in the char.

1. Introduction

Two apparently unconnected problems, reducing dependence on fossil fuels and livestock waste management, may be connected and transformed into opportunities. For decades, Europe has been immersed in trying to reduce energy dependence on external energy sources, as geopolitical instabilities have generated shortages affecting the economy of the 27. A recent example has been the gas supply crisis following the conflict between Russia and Ukraine [1].

Furthermore, Europe is also leading different efforts to decarbonize the economy, aiming to reduce the use of fossil fuels to mitigate global warming. For that purpose, energies rejected in the past, such as nuclear energy, are reconsidered, while other initiatives advocate using renewable energies such as wind or photovoltaic energy. Among these renewable energies is biogas, produced via anaerobic digestion using different raw materials, including agricultural and livestock waste or their mixtures.

Livestock waste in particular is a growing problem in countries like Spain, where in recent years the increase in livestock, specifically in the pig sector, has led to a high manure generation, exceeding in some areas the capacity of the land to assimilate this manure as fertilizer. This creates operational issues for farms due to insufficient land, and even the appearance of environmental problems such as nitrate contamination of aquifers as a result of the over-application and subsequent leaching [2].

Anaerobic digestion is a suitable alternative for the management of livestock and agricultural wastes, and the production of biogas [3], usually through the co-digestion of several feedstocks. Compared to other renewable energy sources, biogas has the advantage of allowing direct injection into the existing natural gas infrastructure, although it has some disadvantages, as will be explained below. Although raw

This article is part of a special issue entitled: Rafael Bilbao published in Biomass and Bioenergy.

* Corresponding author.
E-mail address: isabelfo@unizar.es (I. Fonts).

https://doi.org/10.1016/j.biombioe.2025.107778
Received 22 January 2025; Received in revised form 4 March 2025; Accepted 4 March 2025
Available online 17 March 2025

biogas has a relatively high percentage of methane (CH_4), 50–75 % (v/v), and small amounts of hydrogen (H_2) 0–1 % (v/v), it also has relatively high levels of non-combustible gases, such as carbon dioxide (CO_2) 25–50 % (v/v) or 0–10 % (v/v) nitrogen (N_2), and lower percentages of problematic gases such as hydrogen sulfide (H_2S) 0.1–3 % (v/v) and minimal amounts of other gases [4].

To enhance the fuel quality of biogas by reducing its CO_2 content, and eliminating the problematic component H_2S, adsorption using carbonaceous materials is a promising alternative. Again, this approach brings an opportunity to increase waste utilization, not only to generate biogas, but also to be the precursor of an adsorbent material such as biochar that can be generated via pyrolysis, not from the original waste, but from the solid fraction of the obtained digestate (known as co-digested manure, CDM). This allows a circular use of the waste, minimizing the management required for its by-products.

The use of commercial activated carbon (AC) in biogas upgrading has been the subject of analysis in many scientific works [5–7]. However, some other authors suggest the need for further research into the use of locally available organic waste to produce low-cost CO_2 sorbents, as their utilization will contribute to cost reductions and waste minimization [8]. In this regard, pristine biochar derived from the pyrolysis of waste biomass is a more affordable alternative for biogas conditioning compared to commercial AC. Beyond the large variation of prices that may exist, the average price of pristine biochar produced by pyrolysis is around 400 € t^{-1} on average, which is lower than the average price of AC 1500–2300 € t^{-1}, making biochar an interesting option from an economic point of view.

Similar to AC, whose properties are considerably affected by the raw material used in its production, the properties of biochar are significantly influenced by the composition of the raw material used in its production [9,10]. Due to the low C/N ratio of protein-rich waste, it is common to mix this waste with lignocellulosic residues to increase the methane yield during anaerobic digestion [11,12]. The composition of the digestate differs depending on the substrate digested, although independently it comes only from cow manure or a mixture of manures from different animals, or a mixture of manures and agricultural residues, the most important macrocomponents are cellulose, lignin, proteins, and ash [13–17]; and the substrate only influences in the proportion of these macrocomponents in the digestate, so it is important to deepen into the role of each main macrocomponent in the properties of char as an adsorbent.

Besides the raw feedstock composition, the pyrolysis conditions during biochar preparation, especially the temperature, affect biochar properties directly involved in adsorption, such as microporosity and surface chemistry. Optimizing pyrolysis temperature seems to involve balancing factors such as textural properties, chemical surface functionality, and biochar yield with temperature. Then, it is necessary to maximize the overall performance of biochar production based on the two most influential parameters, the composition of the feedstock and the pyrolysis temperature.

Agricultural wastes, particularly CDM, exhibit significant heterogeneity naturally. Therefore, establishing the relationship between feedstock composition and biochar properties at various pyrolysis temperatures is essential for optimizing the use of these wastes, either individually or as mixtures in co-pyrolysis processes. To date, most of the published scientific literature on pyrolysis of individual macrocomponents is centered on the volatile compounds devolatilized from cellulose and lignin and analyzed by Py-GC/MS [18–20] and on their mechanisms of reaction [18,21], being much rarer than those studying pyrolysis of proteins [22,23]. To a lesser extent, studies about the char structure analyzed by FTIR and NMR and the properties such as of the char product obtained from the pyrolysis of these macro-components can also be found in literature [24–26]. However, properties, such as the pH or the micropore specific surface, which are crucial to assess the applicability of these solid products as adsorbents, are very little studied [24,27]. In this scenario, systematic research needs to be conducted in which the char properties related to the adsorption process obtained from different macrocomponents and at a wide range of pyrolysis temperatures are analyzed. Several works have reported interactions among organic macrocomponents during pyrolysis affecting product yields, as well as the influence of the presence of inorganics in the pyrolysis mechanism affecting product yields and lowering the pyrolysis temperature [28–30]. Hence, studying the effect of these potential interactions among major macrocomponents is crucial for comprehending the effect of feedstock composition on biochar adsorption properties.

In this study, cellulose (CEL), lignin (LIG), soybean protein (SP), and calcium carbonate ($CaCO_3$), have been selected as the primary pure components representative of agricultural wastes, in particular CDM. The presence of $CaCO_3$ in CDM is due to its widespread use as a dietary supplement in animal nutrition, especially in industrial livestock. Each component was individually pyrolyzed to produce biochar. Subsequently, the study was extended to synthesized samples, prepared as a mixture of these components at a ratio close to that found in real CDM. Finally, the analysis was also conducted for a real CDM sample. The specific objectives of this work are as follows: (1) to evaluate the solid properties of the biochars (textural properties, pH, and surface functionalities) and (2) to elucidate the potential interaction effects among the components on biochar properties. The findings of this study provide insights into the effect of the interactions between organic and inorganic components during the pyrolysis of high-ash content waste on biochar properties. This knowledge is particularly relevant for the use of this material as a suitable CO_2 adsorbent as will be shown in Part II of this work.

2. Materials and methods

2.1. Materials

The four selected materials, representing major components of CDM, were used as feedstocks for biochar production, and procured commercially. CEL was sourced from Sigma Aldrich (Sigma Aldrich code C8002). LIG was acquired from J&H Chemical Co. LTD, where the Organosolv process was employed to separate lignin fibers from the rest of the lignocellulosic material. This process involves boiling the material with a mixture of ethanol:water (1:1 vol) at 200 °C for 30 min. For the protein fraction of the CDM, SP was acquired from a drugstore with a stated protein content of 90 %. SP was selected as the protein model component being representative of vegetable proteins likely present in the digested slurry. SP is a mixture of proteins isolated from soybean, with two prominent subunits, β-conglycine (7S) representing 35 % and glycine (11S) representing 52 %. $CaCO_3$, with a stated purity of 99 %, was obtained from Acros Organics and was considered a representative compound for CDM inorganics. The CDM used in this study was provided by the Spanish HTN Biogas Company located in Navarra, where cattle manure is anaerobically co-digested with agro-industry residues and the co-digestate is separated into liquid and solid fractions by centrifugation. Before conducting the experiments, the solid fraction received in our lab was thermally dried overnight at 105 °C in a lab-scale oven, to get the final sample of CDM. The ultimate and proximate analyses of the feedstocks are summarized in Table 1. The Van Soest and the Kjeldahl methods were applied to the CDM sample to determine its content of cellulose, lignin and proteins, with the results presented in Table 1.

Comparison of X-ray Diffraction (XRD) patterns of CDM with those from libraries and quantification of the peaks of the whole spectra by the Rietvel method showed that calcite ($CaCO_3$) was the most abundant crystalline component of the CDM, followed by struvite ($MgNH_4PO_4(H_2O)_6$) and quartz (SiO_2) (see Fig. S1 in Supplementary Information). The CDM used in this study exhibited high ash content, with Ca being the most abundant metal (55.4 g kg^{-1} CDM, dry basis) and P the second one (15.2 g kg^{-1} CDM, dry basis) according to Inductively Coupled Plasma-Atomic Emission Spectroscopy (ICP-AES) analysis (see

Table 1
Characterization of the raw materials used to produce the pyrolysis biochar samples.

Properties	Analytical Standard/ Equipment	CDM	CEL	LIG	SP	$CaCO_3$
Elemental analysis (wt.%, as received)						
Carbon	ISO 16948:2015	29.9 ± 0.1	42.2 ± 0.1	56.7 ± 0.1	46.4 ± 0.1	12.0 ± 0.1
Hydrogen[a]	ISO 16948:2015	4.8 ± 0.1	7.0 ± 0.1	6.1 ± 0.2	7.9 ± 0.1	0
Nitrogen	ISO 16948:2015	2.3 ± 0.1	0	0.9 ± 0.1	13.5 ± 0.1	0
Sulfur	Leco 628 S	0.8 ± 0.1	0	0.2	0.6 ± 0.1	0
Oxygen	by difference[b]	24.8 ± 0.6	50.8 ± 0.1	35.9 ± 0.2	27.4 ± 0.1	–
Proximate analysis (wt.%, as received)						
Moisture	ISO 18134:2021	11.3 ± 0.9	5.3 ± 0.3	21.80 ± 0.02	5.9 ± 0.2	–
Ash[c]	ISO 18122:2016	37.4 ± 0.6	0	1.2 ± 0.1	4.2 ± 0.1	–
Volatiles	ISO 18123:2016	49.7 ± 0.7	94.7 ± 0.3	67.9 ± 0.1	80.8 ± 0.4	–
Fixed Carbon	by difference[d]	1.6 ± 0.9	–	9.1 ± 0.1	9.1 ± 0.5	–
Organic macro-components (wt.%, as received)						
Cellulose	Van Soest	26.9 ± 0.4	–	–	–	–
Lignin	Van Soest	17.1 ± 0.1	–	–	–	–
Proteins	Van Soest	11.7	–	–	–	–

[a] Hydrogen content includes hydrogen from moisture.
[b] Oxygen was calculated by difference according to: O(wt.%) = 100-C(wt.%)-H(wt.%)-N(wt.%)-S(wt.%)-Ash(wt.%).
[c] Ash was determined as the mass of solid remaining after heating the sample at 550 °C in air at strict timing conditions.
[d] Fixed carbon was calculated by difference according to: Fixed carbon(wt.%) = 100-Moisture(wt.%)-Volatiles(wt.%)-Ash(wt.%).

Table S1 in Supplementary Information). Based on the composition of the CDM (organic macro-components concentration and inorganic composition and concentration) and assuming that all the Ca is as $CaCO_3$, a synthetic sample simulating CDM (Surrogate_CDM) was prepared using 39 wt% of CEL, 24 wt% of LIG, 17 wt% of SP and 20 wt% of $CaCO_3$. Surrogate_CDM was prepared by mixing in a perfect way the exact amount of each macro-component required to achieve the aforementioned concentrations in a final mass of 10 g. The whole mixture was introduced in the reactor. The particle size of the materials used as feedstocks was <150 μm.

The procedure for biochar production has been detailed elsewhere [31], although in this work the reactor used has a higher capacity (around 10 g). In brief, pyrolysis experiments were conducted in a fixed-bed reactor with 5–10 g capacity at three different temperatures (350, 550 or 750 °C) with a heating rate of 10 °C min^{-1}, maintaining the final temperature for 1 h. The reactor, constructed of stainless steel, was positioned inside an electrically heated oven capable of reaching the desired temperature. A flow of 45 cm^3STP min^{-1} of N_2 was used as a carrier gas to ensure an inert atmosphere in the reactor. The nitrogen flow was maintained also during the cooling phase of the reactor to prevent the entry of atmospheric air. The difference in weight of the reactor tube before and after the experiment was utilized to calculate the solid product yield. Between 3 and 5 replicates of experiments were conducted at each temperature to assess the experimental variability. The experimental results are presented as mean ± standard deviation. The biochar samples are designated as the abbreviation of the raw material used (CEL, LIG, SP, $CaCO_3$, CDM, Surrogate_CDM) followed by a number indicating the final pyrolysis temperature. For example, CEL350 refers to the biochar prepared by cellulose pyrolysis at 350 °C.

2.2. Char characterization

The biochar samples used in this study were characterized by different methods. Elemental analysis (C, H, N, and S content) was determined using the CHNS Analyzer (LECO CHN 628 and LECO S TruMac Series Elemental Analyzer). The pH of the biochar samples was determined following the procedure by Ref. [32], wherein pH was measured in a solution of biochar in deionized water (1:20 w:v) after agitation for 1 h. Surface functional groups on the biochar surface were identified via Attenuated Total Reflection-Fourier Transform Infra-Red (ATR-FTIR) spectroscopy analysis, conducted using an Agilent Cary 600 FTIR spectrometer with a resolution of 4 cm^{-1} in the wavenumber range of 4000-400 cm^{-1}. X-ray photoelectron spectroscopy (XPS) employing a Kratos Axis Supra XPS spectrometer with a monochromatic Al Kα X-ray source (photon energy; 1486.6 eV) was used to characterize the elemental and chemical composition of the very top surface (1–10 nm) of the biochar samples. The binding energy scale was standardized by the C1s peak at 284.6 eV.

The surface morphology characteristics of the biochar adsorbents were obtained by a Scanning Electron Microscope (SEM) using a JEOL JSM-6400 microscope, with accelerating voltages ranging from 2.0 to 40 kV. The textural properties of char, including specific surface area (SS), pore volume, and pore size distribution (PSD) were evaluated by adsorption and desorption test with N_2 and CO_2 at 77 K and 273 K, respectively, using an Autosorb-iQ3 (Quantachrome Instruments). Before the experiments, the samples underwent vacuum outgassing at 200 °C for 900 min. The apparent specific surface area (SS_{BET}) of the biochar was calculated using the Brunauer-Emmett-Teller (BET) equation and the t-plot method was employed to estimate the micropore volume ($V_{micro\text{-}BET}$) using the N_2 isotherm at low relative pressures ($P_{N_2}/P_{0\ N_2}$ = 0.05–0.2). The specific surface area (SS_{DR}) and micropore volume ($V_{micro\text{-}DR}$) were determined by the Dubinin-Radushkevich (DR) model using the isotherm of CO_2. Additionally, the cumulative volume for various pore size ranges (V_{micro}<0.5 nm, 0.5 nm < V_{micro}<0.8 nm and 0.8 nm < V_{micro}<1.5 nm) was obtained using Non-Local Density Functional Theory (NLDFT) for slit-shaped pores using the CO_2 isotherm.

2.3. Interaction effects calculation

The interaction effects appearing due to the simultaneous presence of different macro-components have been studied for biochar yield and biochar properties related to its textural and chemical characteristics. To check potential interaction effects among the biomass components on the aforementioned response variables, the experimental data for the Surrogate_CDM were compared to the theoretical values (Theo_CDM). These theoretical values represent the expected values in the absence of interaction effects, assuming the additive proportional contribution of each component based on its proportion. The theoretical biochar yield for CDM ($\eta_{char_{theo\_CDM}}$) (wt.%), calculated using Eq. (1), represents the yield expected during the pyrolysis of Surrogate_CDM in the absence of interaction effects; x_i is the concentration (wt.%) of each component in Surrogate_CDM (39 wt% of CEL, 24 wt% of LIG, 17 wt% of SP and 20 wt % of $CaCO_3$); η_{char_i} is the experimentally determined biochar yield (wt. %) for each individual component (CEL, LIG, SP, $CaCO_3$).

$$\eta_{char_{theo\_CDM}}(wt.\%) = \sum \frac{x_i\ (wt.\%)}{100} \cdot \eta_{char_i}\ (wt.\%) \qquad \text{Eq. 1}$$

Theoretical values for the response variables (RV) referring to the chemical and physical characterization of biochar were calculated using Eq. (2), where $RV_{char_{theo\_CDM}}$ is the theoretical value of the property for Surrogate_CDM biochar assuming no interaction effects; RV_{char_i} denotes the experimental value of the property for the biochar produced from "i" macro-component; $Contribution_{char_i}$ is the percentage contribution of each macro-component to the final biochar yield calculated using Eq.

(3). This contribution differs from its concentration (x_i) in the raw Surrogate_CDM (before pyrolysis), as the experimental biochar yield of each macro-component varies depending on the pyrolysis temperature (see Table 2).

$$RV_{char_{theo\_CDM}} = \sum \frac{Contribution_{char_i}\ (\%)}{100} \cdot RV_{char_i} \quad \text{Eq. 2}$$

$$Contribution_{char_i}(\%) = \frac{\frac{x_i\ (wt.\%)}{100} \cdot \eta_{char_i}\ (wt.\%)}{\sum \frac{x_i\ (wt.\%)}{100} \cdot \eta_{char_i}\ (wt.\%)} \times 100 \quad \text{Eq. 3}$$

To assess the interaction effects between components, a t-student test with a significance level of 0.05 was applied to compare the experimental values of biochar yields and characterization obtained from Surrogate_CDM and their theoretical values calculated for Theo_CDM using Eqs. (2) and (3). If significant interaction effects were observed ($p_{value}<0.05$), the interaction effect (IE) was quantified using Eq. (4). A positive IE indicates a synergistic effect among the components, whereas a negative value indicates an antagonistic effect.

$$IE\ (\%) = \frac{RV_{char_{surrogate\_CDM}} - RV_{char_{theo\_CDM}}}{RV_{char_{theo\_CDM}}} \times 100 \quad \text{Eq. 4}$$

3. Results and discussions

3.1. Char yield pyrolysis

The biochar yields obtained experimentally from the CDM, its four components (CEL, LIG, SP, $CaCO_3$) and the Surrogate_CDM at the three pyrolysis temperatures are shown in Table 2, along with the theoretical values that would be obtained with the Surrogate_CDM if there were no interactions (Theo_CDM). As expected, an increase in the pyrolysis temperature led to a decrease in the biochar yield for the organic macro-components (CEL, LIG and SP) and the CDM, due to an increase in the decomposition rate of organic matter. This decrease was particularly pronounced between 350 and 550 °C for the organic macro-components. However, for $CaCO_3$, CDM and Surrogate_CDM a clear reduction between 550 and 750 °C was observed. $CaCO_3$ decomposition, under the experimental conditions of this work, starts to be noticeable in the temperature range of 550–750 °C, which could also explain the biochar yield decrease in CDM and Surrogate_CDM between 550 and 750 °C. Among the organic macro-components, LIG yielded the highest biochar since its structure is highly thermal stable. The higher biochar yield obtained from LIG than from CEL is due to the lower concentration in volatiles and the higher in fixed carbon of lignin, and is consistent with the results from the literature [33]. Higher biochar yields are of interest since it means that more biochar will be available for being used as a solid adsorbent. The high inorganic fraction in CDM explains its relatively higher biochar yield in comparison with those from CEL and LIG, due to the scarce thermal decomposition of the inorganic fraction for the whole temperature range studied.

To study the possible interaction effects between components, the experimental biochar yields obtained from the Surrogate_CDM were compared to the theoretical biochar yields (Theo_CDM) calculated as the weighted average considering the composition of the Surrogate_CDM and the experimental biochar yields obtained for the individual macro-components pyrolyzed separately (see Eq. (2)). As shown in Table 2, the biochar yields obtained experimentally for the Surrogate_CDM and those calculated for the Theo_CDM are different ($p_{value} < 0.05$) for the three pyrolysis temperatures, which could reveal interaction among components during pyrolysis. The biochar yields obtained at 350 °C and 550 °C for the Surrogate_CDM were higher than the expected ones (Theo_CDM350 and Theo_CDM550), suggesting a synergetic effect (IE = 18 % and 8 %, respectively). However, at 750 °C, the interaction effect is antagonist (IE = −14 %), resulting in a biochar yield lower than expected. The addition of inorganic substances to biomass tends to increase biochar yields [34], as could explain the results obtained in this

Table 2
Experimental data of char yield, elemental analysis and pH of raw materials and biochar samples prepared by pyrolysis at different temperatures. Calculated data for Theo_CDM.

	Char yield (wt%)	C (wt %)	H (wt %)[a]	N (wt %)	S (wt %)	pH
CEL	–	42.2 ± 0.1	7.0 ± 0.1	0.2 ± 0.1	0	7.34 ± 0.04
CEL350	26 ± 2	71.4 ± 0.1	4.2 ± 0.1	0	0	6.82 ± 0.02
CEL550	18 ± 2	88.2 ± 0.2	3.0 ± 0.1	0	0	7.8 ± 0.3
CEL750	17 ± 2	92.8 ± 0.6	1.6 ± 0.1	0	0	8.1 ± 0.1
LIG	–	56.7 ± 0.1	6.1 ± 0.2	0.9 ± 0.1	0.21 ± 0.02	3.54 ± 0.01
LIG350	48 ± 1	68.7 ± 0.9	4.5 ± 0.1	1.1 ± 0.1	0.17 ± 0.02	7.19 ± 0.04
LIG550	34 ± 1	82.9 ± 0.1	3.2 ± 0.1	1.2 ± 0.1	0.13 ± 0.02	8.1 ± 0.02
LIG750	34 ± 4	86.7 ± 0.01	2.2 ± 0.1	1.0 ± 0.1	0.17 ± 0.03	8.52 ± 0.03
SP	–	46.4 ± 0.1	7.9 ± 0.1	13.5 ± 0.1	0.6 ± 0.1	6.59 ± 0.02
SP350	41 ± 4	59.5	4.4	12.1	0.14 ± 0.01	9.17 ± 0.09
SP550	27 ± 1	56.9 ± 0.2	2.8 ± 0.1	10.4 ± 0.1	0.10 ± 0.01	9.72 ± 0.08
SP750	24 ± 3	62.3 ± 0.1	1.6 ± 0.1	9.2 ± 0.1	0.05 ± 0.01	9.99 ± 0.02
$CaCO_3$	–	12.0 ± 0.1	0	0	0	9.77 ± 0.05
$CaCO_3$350	99.1 ± 0.3	12.0 ± 0.1	0	0	0	9.65 ± 0.04
$CaCO_3$550	99.3 ± 0.3	11.7 ± 0.2	0	0	0	9.85 ± 0.09
$CaCO_3$750	92.4 ± 0.7	11.1 ± 0.6	0	0	0	12.6 ± 0.1
CDM	–	29.9 ± 0.1	4.9 ± 0.1	2.2 ± 0.1	0.8 ± 0.1	7.61 ± 0.01
CDM350	59 ± 1	37.4 ± 0.3	2.3 ± 0.1	2.5 ± 0.1	1.03 ± 0.01	7.74 ± 0.04
CDM550	51 ± 3	35.0 ± 0.5	1.5 ± 0.1	1.0 ± 0.2	1.18 ± 0.04	9.7 ± 0.1
CDM750	42 ± 1	33.8 ± 0.4	1.0 ± 0.1	0.6 ± 0.1	1.49 ± 0.05	12.7 ± 0.1
Surrogate_CDM[b]	–	40.4	5.5	2.6	0.15	6.8
Surrogate_CDM350	57 ± 4	47.1 ± 0.2	3.1 ± 0.1	3.0 ± 0.1	n.d.	9.29 ± 0.03
Surrogate_CDM550	42 ± 1	48.8 ± 0.1	1.8 ± 0.1	2.6 ± 0.1	0.03 ± 0.03	9.35 ± 0.08
Surrogate_CDM750	32 ± 2	49.8 ± 0.1	1.8 ± 0.1	2.0 ± 0.1	0.08 ± 0.01	12.5 ± 0.1
Theo_CDM[b]	–	40.4 ± 0.2	5.5 ± 0.2	2.6 ± 0.2	0.2 ± 0.1	6.8
Theo_CDM350	48 ± 4 IE = 18 %	44.8 ± 0.9 IE = 5 %	2.6 ± 0.2 IE = 19 %	2.0 ± 0.1 IE = 50 %	0.02 ± 0.01[c]	8.4 ± 0.1 IE = 11 %
Theo_CDM550	39 ± 2 IE = 8 %	45.2 ± 0.3 IE = 8 %	1.5 ± 0.2[c]	1.6 ± 0.1 IE = 73 %	0.01 ± 0.01[c]	9.1 ± 0.1[c]
Theo_CDM750	37 ± 4 IE = −14 %	47.6 ± 0.8 IE = 4 %	0.9 ± 0.2 IE = 100 %	1.2 ± 0.1 IE = 67 %	0.01 ± 0.01[c]	10.6 ± 0.1 IE = 18 %

n.d.: not determined.
[a] Hydrogen content includes hydrogen from moisture.
[b] Calculated from the elemental composition of the raw individual components.
[c] Interaction effect was not evidenced.

work at 350 and 550 °C. Calcium could catalyze some re-polymerization reactions of the tar products, favoring biochar formation [35]. However, the significantly lower biochar yield for the Surrogate_CDM750 than for the Theo_CDM750 could be due to two different causes: (i) firstly, the thermal decomposition of the $CaCO_3$ could begin at lower temperatures in the presence of organic constituents than when it is pyrolyzed separately due the presence of acids [36]; the acids resulting from the pyrolysis of cellulose would be present in the pyrolysis liquid intermediate [37] favoring the decomposition of $CaCO_3$; (ii) subsequently, the presence of CO_2 coming from the thermal decomposition of $CaCO_3$ could promote the reverse Boudouard reaction ($C(s) + CO_2(g) \leftrightarrow 2CO(g)$), hereafter simply Boudouard reaction, between the aforementioned CO_2 and the carbon present in the char, reducing the biochar yield. The promotion of the Boudouard reaction during Surrogate_CDM pyrolysis as a consequence of the higher CO_2 concentration has been evidenced by the significantly much higher CO yields obtained during the pyrolysis of Surrogate_CDM at 750 °C compared to those obtained from theoretical calculation (IE = 190 %). In addition, CDM pyrolysis also generated higher CO_2 and CO yields compared to those obtained from the pyrolysis of the organic macro-components at 750 °C (see Table S2 in Supplementary Information for CO yield data).

3.2. Char characterization

To compare the properties of the biochar produced from the Surrogate_CDM with those that would theoretically (Theo_CDM char) arise from the summative proportional contribution of the macro-components pyrolyzed individually, the theoretical $Contribution_{char_i}$ (%) shown in Eq. (3) has been calculated and are shown in Table 3. Subsequently, the biochar properties of these Theo_CDM biochar samples were calculated according to Eq. (2).

3.2.1. Elemental composition

The elemental analysis of both the raw materials and the biochar samples is presented in Table 2. Compared with the carbon content of the raw materials, the biochar products from the three organic macro-components (CEL, LIG, and SP), as well as the biochar products from CDM and Surrogate_CDM, exhibited higher carbon contents. As expected, following a pyrolysis treatment [38], the carbon content of the chars obtained from CEL, LIG, and Surrogate_CDM increased with rising pyrolysis temperature. Other authors have also found char samples from CEL present higher C contents than those from LIG [24]. However, the carbon content of the SP chars reached a minimum at 550 °C, while that of the CDM chars decreased across the entire pyrolysis temperature range studied (350–750 °C). Regarding the carbon content of the solids obtained from the inorganic macro-component studied ($CaCO_3$), a decreasing trend with the temperature was observed, possibly due to partial decomposition into CaO that remains in the solid, while carbon content is lost in the form of CO_2 that would be released from the solid matrix during pyrolysis. The effect of the temperature on the decrease of the carbon content of the solid samples was more significant for those solids obtained from CDM than for those obtained from $CaCO_3$, supporting the idea of earlier $CaCO_3$ decomposition in the presence of organic constituents and, consequently, the promotion of the Boudouard reaction between the CO_2 from the decomposition and the carbon present in the char.

Table 3
Theoretical contribution of the biochar of each macro-component to the Theo_CDM biochar samples ($Contribution_{char_i}$ (%)).

$Contribution_{char_i}$ (%)	Theo_CDM350	Theo_CDM550	Theo_CDM750
CEL	21.0	17.7	17.6
LIG	23.9	20.6	21.8
SP	14.2	11.6	11.1
$CaCO_3$	40.9	50.1	49.5

The biochar samples obtained from SP were notably richer in nitrogen (N) than those from the other macro-components. CDM biochar samples contained higher concentrations of both N and sulfur (S) than typical lignocellulosic biomass chars, as raw lignocellulosic biomass contain negligible N and S compared to the CDM. The presence of N and S in CDM chars was attributed to proteins coming from the raw manure itself and also microorganisms involved in anaerobic digestion. As the pyrolysis temperature increased, the S content of the SP and Surrogate_CDM chars decreased dramatically compared to the S content in the raw material, while the S content of the CDM chars increased. This behavior suggests that S in CDM does not only come from the protein fraction but also from the inorganic fraction. S content in raw CDM was similar to that of SP despite the protein fraction in CDM represents only 12 wt% of the sample. So, if S only comes from proteins, CDM should contain as much as 0.1 wt% instead of 0.8 wt% (see Table 1).

It was observed that the elemental compositions of the Surrogate_CDM chars differed significantly ($p_{value} < 0.05$) from those that would be theoretically obtained at any of the pyrolysis temperatures (see Table 2), pointing to a possible interaction effect similar to what was observed with biochar yield. The elements analyzed (C, H, N, and S) exhibited higher concentrations in the chars obtained from Surrogate_CDM compared to those theoretically expected. The highest IE were observed for N content. Some authors claim that O-containing groups in chars, such as carbonyls from cellulose, could potentially react with NH_3, NH_2 and NH through Maillard reactions forming N-containing groups (pyridinic-N, pyrrolic-N, quaternary-N and pyridone-N-oxide), thereby favoring the retention of N in the biochar [39]. Therefore, co-pyrolysis of lignocellulosic wastes with rich protein wastes could enhance biochar nitrogen retention affecting the pH and surface functionality in chars, which in turn might influence their CO_2 adsorbent performance [39]. However, the N content in the biochar from CDM decreased with temperature more significantly than for Surrogate_CDM, indicating no significant N retention in CDM despite the presence of O and N-containing groups. This observation could be attributed to the fact that the N contained in CDM does not solely originate from the protein fraction.

3.2.2. pH

The pH values of the raw materials ranged from 3.5 to 9.8, while the pH of the biochar samples varied between 6.8 and 12.8, as shown in Table 2. Moreover, the pH of the biochar samples produced from all the raw materials (CEL, LIG, SP, $CaCO_3$ and DCM) increased with the pyrolysis temperature. Similar trends were reported in the literature for lignocellulosic biochars, which was attributed to the reduction in acidic functional groups, such as hydroxyl and carboxylic, during the pyrolysis [40]. In addition to the removal of carboxylic functional groups, the increased basicity of CEL750 and LIG750 may result from an increase in Lewis basic sites on the biochar surface. According to Li et al. [40], removing oxygen from the carbon surface can delocalize free electrons on the carbon surface's basal planes, enabling them to behave as Lewis basic sites. An exception to this behavior is the CEL350 biochar sample, which exhibited a lower pH than the raw CEL, suggesting the presence of more acidic groups. Peaks in the range of 1600–1800 cm^{-1}, assigned to carboxylic acids (1665-1760 cm^{-1}) and lactones (1675-1790 cm^{-1}), were observed in the CEL350 biochar but not in the FTIR spectrum of the raw CEL. The FTIR spectra for the raw materials and biochar samples are shown in Figs. S2–S6 in the Supplementary Information. Matsuoka et al. [41] proposed that during the initial stages of pyrolysis, the thermal decomposition of reducing end groups in crystalline cellulose could enable proton donation (acting as an acid catalyst). This proton donation through hydrogen bonding between surface biochar functional groups plays a fundamental role in these pyrolytic reactions, leading to the formation of more acidic groups.

SP chars exhibited higher pH values than biochar derived from other organic macro-components, likely due to the presence of pyridinic-N and pyrrolic-N functionalities formed on the biochar surface during

pyrolysis from the transformation of the N functionalities present in raw SP. SP contains a significant concentration of N originating from typical N-functionalities in proteins, such as amine (side-chain) and amide (peptidic bond) [42]. XPS spectra of SP chars revealed that N-functionalities in raw SP primarily transformed into pyridinic-N and pyrrolic-N, both showing basic characteristics as they can act as Lewis base sites. Additionally, XPS spectra revealed a higher concentration of N on the surface of SP-derived chars than those from CEL or LIG, possibly explaining the higher pH of SP chars. Pyridinic-N exhibits higher basicity than pyrrolic-N, as its electron lone pair is not part of the aromatic ring [43]. Deconvolution of N 1s XPS spectra of SP chars (see Fig. S2 in Supplementary Information) indicated a significant increase in the percentage of pyridinic-N (398.7 ± 0.1 eV) in the biochar produced at 550 (36 %) vs. the biochar produced at 350 °C (25 %), justifying the higher basicity of SP550. The pH of SP750 was slightly higher than that of SP550. This pH increment was not attributed to a greater presence of pyridinic-N, as its percentage was lower in SP750 (20 %) than in SP550 (36 %) (see Table S3 in Supplementary Information); this increase may instead be related to changes in the carbonaceous structure, similar to those observed on CEL and LIG.

The pH of the solid samples obtained from $CaCO_3$ thermal decomposition was basic, consistent with that of the $CaCO_3$ itself, as it suffers minimal decomposition at 350 and 550 °C. The higher pH value recorded for the $CaCO_3$750 sample could be explained by the partial decomposition of $CaCO_3$ into CaO, which exhibits a stronger basic character than $CaCO_3$. The results of FTIR spectra of $CaCO_3$ and its biochar samples support this explanation (see Fig. S3). The increase in pH values for CDM and Surrogate_CDM biochar samples with the pyrolysis temperature may be attributed to the growing presence of Lewis base sites and the partial decomposition of the $CaCO_3$ present in the inorganic fraction of CDM. Interaction of CO_2 with basic biochar functionalities is feasible due to the acidic nature of CO_2 [44]. Higher pyrolysis temperature in the studied range (350–750 °C) seemed suitable for generating biochar with basic characteristics, especially for feedstocks with high protein content.

When comparing the pH of biochar samples derived from Surrogate_CDM to the theoretically expected values (Theo_CDM) calculated from the weighted average of biochar samples pH from macrocomponents (see Table 2), an important synergistic effect (IE = 18 %) was observed in the pH of the Surrogate_CDM750 sample. The significantly higher basic character of Surrogate_CDM750 (12.5) compared to the theoretical one, Theo_CDM750 (10.6), could be caused by the promotion of $CaCO_3$ thermal decomposition in the presence of the organic constituents during pyrolysis. As mentioned earlier (see Section 3.1), the decomposition of $CaCO_3$ is likely promoted by the presence of acid groups in the liquid intermediate formed in the pyrolysis of cellulose.

3.2.3. Morphology

The scanning electron microscope (SEM) images of CEL750, LIG750, SP750, CDM750, and Surrogate_CDM750 are shown in Fig. 1 and the SEM images of char samples obtained at 350 and 550 °C are shown in Fig. S8 in Supplementary Information. LIG750 and SP750 chars displayed individual particles with polygonal shapes and multiple smooth surfaces, although some pores can be observed in the SEM image of LIG750. The smooth surfaces could result from the solidification of a liquid intermediate formed during the pyrolysis of LIG and SP (melting stage). SEM images of LIG350 and SP350 (see Fig. S8) already showed biochar particles with smooth surfaces, indicating that these liquid intermediates should be formed even at temperatures lower than 350 °C. In contrast, biochar samples from CEL, Surrogate_CDM, and CDM showed rougher surfaces across all pyrolysis temperatures studied. Comparing the SEM image of Surrogate_CDM750 and CDM750, different components can be distinguished in Surrogate_CDM750 indicating a lower degree of intimate contact between them.

3.2.4. Textural characterization of char

Table 4 shows the specific surface areas obtained by the Brunauer-Emmett -Teller (BET) and Dubinin-Radushkevich (DR) methods for N_2 at 77 K and CO_2 at 273 K adsorption, respectively. Except for CEL550 and CEL750, the specific surface area of the chars obtained by BET method with N_2 were below 100 m^2/g. Other authors have found that BET specific surface area is higher for chars from delignified oak wood than for chars obtained from raw oak [45], pointing out also to cellulose as a better precursor for high-specific surface areas. However, when applying the DR method to the adsorption data of CO_2 at 273 K, the specific surface area of all biochar samples increased significantly

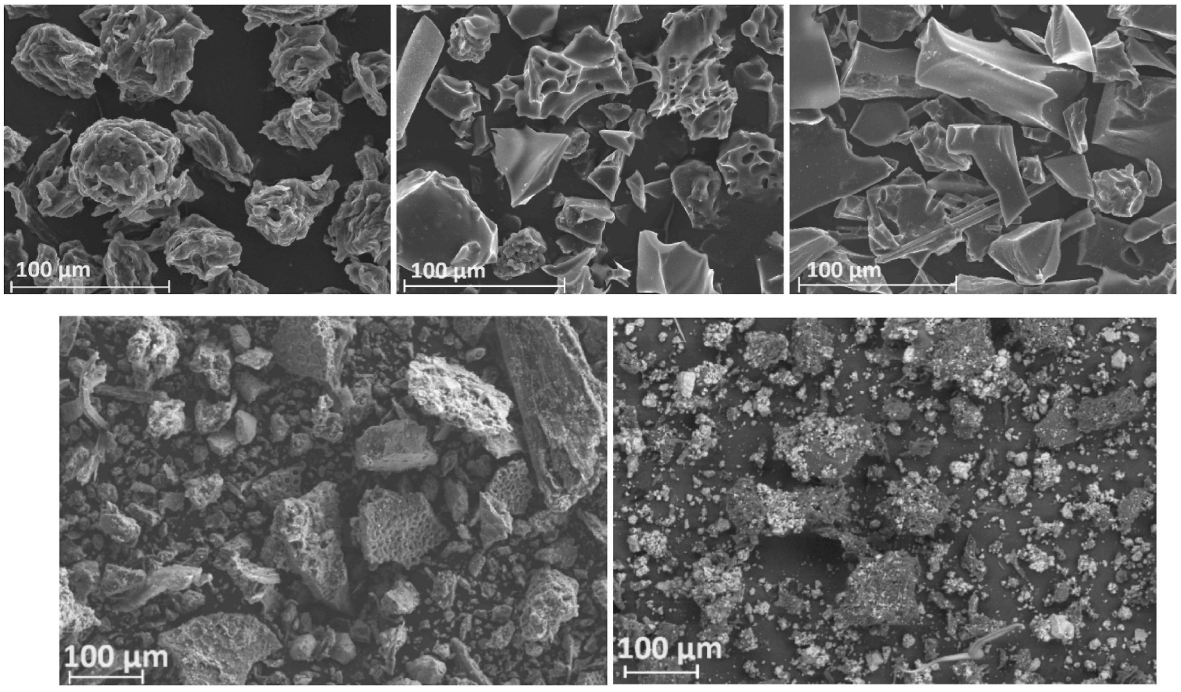

Fig. 1. Scanning electron microscopes (SEM) image of (a) CEL750, (b) LIG750, (c) SP750, (d) CDM750 and Surrogate_CDM750 (scale of 100 µm).

Table 4
Textural properties of chars determined from N2 adsorption at 77 K and CO2 adsorption at 273 K.

	N_2 adsorption at 77 K	CO_2 adsorption at 273 K	
	SS_{BET} ($m^2\ g^{-1}$)	SS_{DR} (m^{2-1})	V_{DR} ($cm^3\ g^{-1}$)
CEL350	6	311	0.12
CEL550	298	562 ± 21	0.211 ± 0.008
CEL750	352	704 ± 31	0.26 ± 0.01
LIG350	2	271	0.10
LIG550	26	536 ± 32	0.20 ± 0.01
LIG750	61	648	0.24
SP350	5	132	0.05
SP550	5	268 ± 8	0.101 ± 0.004
SP750	1	222	0.08
$CaCO_3$350	n.d.	n.d.	n.d.
$CaCO_3$550	n.d.	42	0.02
$CaCO_3$750	3	89	0.03
CDM350	6	80	0.03
CDM550	16	198 ± 41	0.07 ± 0.02
CDM750	84	248 ± 19	0.093 ± 0.007
Surrogate_CDM350	5	155	0.06
Surrogate_CDM550	48	259	0.097
Surrogate_CDM750	51	357 ± 1	0.127 ± 0.001
Theo_CDM350	2	151	0.06
Theo_CDM550	81	241	0.08
Theo_CDM750	75	289	0.11

compared to the BET values obtained for N_2 at 77 K. This shows an important presence of micropores and ultramicropores in the biochar samples obtained from all these materials, as CO_2 molecules can diffuse more easily into small pores at a higher temperature (273 K) [46]. The much higher SS_{DR} determined from the standardized CO_2 adsorption test than the SS_{BET} determined from the standardized N_2 adsorption test agrees with results obtained in other works for lignocellulosic chars [47], which points to the CO_2 adsorption test and the Dubinin-Radushkevich equation as more appropriate for the analysis of the specific surface area of this type of sample. Biochar samples from CEL and LIG exhibited higher surface areas than those from SP. The melting step during SP pyrolysis seems to hinder the development of microporosity in SP chars, as observed in the SEM images. SEM images have shown that the melting stage in the soybean protein takes place at temperatures between 200 and 250 °C (see Fig. S9) and that the smooth aspect of the surface of the protein char is also maintained for the chars obtained at 350, 550, and 750 °C (see Fig. 1).

CDM chars exhibited a lower surface area than that of the chars from the organic constituents. The absence of porosity in the solids resulting from $CaCO_3$ thermal decomposition, along with its high concentration in CDM char, could justify the lesser development of high surface area and even might fill or block the access to micropores in CDM chars. Different authors also have found that high ash contents limit the development of porosity in biochar samples [48] or which is the same, a greater development of the volume of micropores of the solids was observed as the burn-off of said solids increased [46]. The DR specific surface (SS_{DR}) of CEL and LIG chars increased with the temperature within the studied interval due to the degradation of organic matter, which promotes micropore formation. However, the SS_{DR} of SP chars peaked at 550 °C. Therefore, while the general observed trend for cellulose- and lignin-rich agricultural wastes is that surface area and micropore volume increased with increasing pyrolysis temperature in the range 350–750 °C, protein-rich wastes appear to show a maximum at an intermediate value in this temperature range.

The SS_{DR} obtained in this work for pristine biochar from CEL and LIG at 750 °C is in the same range or even higher as those obtained in other works for physically activated carbon (289–610 cm^2g^{-1}) [49,50], (426–526 cm^2g^{-1}) [51]. In the same way, the micropore volume ($V_{micro,DR}$) of the chars from CEL and LIG obtained at the highest temperature (0.24–0.26 $cm^3(STP)g^{-1}$) (see Table 4) is similar to those reported by other authors for physically activated chars (0.12–0.21 $cm^3(STP)g^{-1}$) [49,52] or (0.12–0.40 $cm^3(STP)g^{-1}$) [53].

Fig. 2 shows the pore volume for three ranges of pore widths (0.3 nm < pore width <0.5 nm, 0.5 nm < pore width <0.8 nm, 0.8 nm < pore width <1.5 nm) as obtained by the NLDFT method. In general, the micropore volume across all pore width ranges was higher for biochar samples derived from CEL and LIG than those from the other raw materials pyrolyzed at the same temperature. For all biochar samples, the micropore volume of smaller pores increased with higher pyrolysis temperatures. According to Presser et al. [54], during CO_2 adsorption at ambient temperature and at 1 bar of CO_2 partial pressure, pores smaller than 0.8 nm (but bigger than 0.5 nm) contribute most to CO_2 uptake, while CO_2 adsorption in pores smaller or equal to 0.5 nm occurred at 0.1 bar. Considering this conclusion, chars from CEL750 and LIG750 are expected to have the highest CO_2 adsorption capacities at the CO_2 partial pressures studied (0.01–0.83 bar), as will be shown in Part II of this work [*reference*].

A positive interaction effect was observed when comparing the micropore volume for the Surrogate_CDM750 sample with the theoretical value (Theo_CDM). As mentioned earlier, the accelerated thermal decomposition of $CaCO_3$ in the presence of the organic components during pyrolysis could generate CO_2 which further reacts with the carbon skeleton, forming CO and new pores. Regarding this result, Jalalabadi et al. also found that carbonate is involved in the cracking of condensable volatiles, which generates a highly porous char structure [55]. The ultramicropore volume, particularly for pores smaller than 0.5 nm, increased beyond the theoretically expected value for the Surrogate_CDM750.

4. Conclusions

The effect of pyrolysis temperature on the chemical and textural properties of the biochar samples is consistent across many raw materials and properties. For instance, the pH and specific surface area, both BET and Dubinin-Radushkevich, increase with temperature, whereas biochar yield and hydrogen content decrease as the temperature increases. The only discrepancy observed is the decrease of specific surface area in the soybean char obtained at 750 °C due to a thermoplastic stage during which the protein melts and re-solidifies, as evidenced by SEM images. Only some properties show temperature-dependent trends that vary with the feedstock precursor. In this regard, the carbon content increases with pyrolysis temperature for cellulose, lignin and soybean protein chars, whilst it decreases for solids derived from the thermal

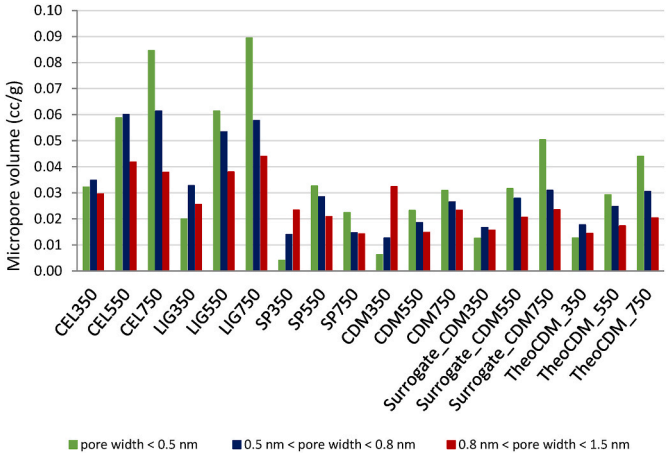

Fig. 2. Micropore volume distribution obtained using the NLDFT method by standardized adsorption of CO_2 at 273 K.

decomposition of $CaCO_3$ and co-digested manure (CDM) due to the thermal decomposition of carbonate.

Based on the mechanism of CO_2 adsorption over pristine biochars, the analysis of standard CO_2 adsorption isotherms at 273 K using the Dubinin-Radushkevich equation, along with the use of the non-local density functional theory (NLDFT) to determine the micropore size distribution are really useful techniques to characterize ultra-microporosity and estimate the CO_2 adsorption performance of these biochars. High-temperature pyrolysis (750 °C) chars coming from lignin- and cellulose-rich residues exhibit micropore specific surface area and volume similar to physically activated carbon, which is an advantage from an operational (due to simplicity) and an economic point of view.

Evidence of the occurrence of interactions between the macro-components of biogenic waste during their co-pyrolysis have been found in this work. Maillard reactions between cellulose and protein fractions cause greater than expected N retention in the resulting char. Organic wastes with high $CaCO_3$ content in their ash, such as CDM, may exhibit interaction effects between their organic and inorganic fractions during pyrolysis. Solid derived from $CaCO_3$ pyrolysis exhibits minimal values of porosity, resulting in very low specific surface area in char produced from wastes with high $CaCO_3$ content. However, at high temperatures (>750 °C), $CaCO_3$ thermal decomposition is favored by the co-pyrolysis of the organic components, probably caused by decomposition products from cellulose. The CO_2 released during this decomposition promotes the Boudouard reaction, leading to a reduced char yield from the organic constituents. Besides this lower biochar yield, this interaction results in a higher ultramicropore and micropore volume of the resulting biochar. However, this synergistic effect is insufficient to counterbalance the dilution effect observed in residues with high ash content. These findings, along with the differences observed between the chars produced from surrogate co-digested manure (CDM) (prepared as a combination of these components) and the theoretical calculations, based on the experimental yields and properties of chars from pure macro-components, prompt further investigation into the interactions among the major constituents of CDM to better understand their combined effects.

During the preparation of this work the authors used Grammarly Inc. add-in (free version) for Microsoft Office in order to check grammatical errors in the text. After using this tool, the authors reviewed and edited the content as needed and take full responsibility for the content of the publication.

CRediT authorship contribution statement

África Navarro: Methodology, Investigation, Formal analysis, Data curation. **Isabel Fonts:** Writing – review & editing, Writing – original draft, Conceptualization. **Joaquín Ruiz:** Writing – review & editing, Methodology, Formal analysis, Data curation. **Jesús Ceamanos:** Writing – review & editing, Supervision. **Noemí Gil-Lalaguna:** Writing – review & editing, Supervision, Formal analysis. **María Benita Murillo:** Writing – review & editing. **Gloria Gea:** Writing – review & editing, Writing – original draft, Supervision, Funding acquisition, Formal analysis, Conceptualization.

Acknowledgements

The authors express gratitude for providing frame support for this work to the Project PID2022-137016OB-I00 financed by Ministerio de Ciencia, Innovación y Universidades and Agencia Estatal de Investigación (MICIU/AEI)/10.13039/501100011033, Spain and by FEDER, UE. Aragón Government has also given frame support (Research Group Ref. T22_23R). I. Fonts acknowledges the post-doctoral fellowship (RYC2020-030593-I) financed by MICIU/AEI/10.13039/501100011033 and by El FSE invierte en tu futuro. A. Navarro-Gil acknowledges the FPI help received (PRE2020-093382) financed by MICIU/AEI/10.13039/501100011033 by "FEDER/UE". The authors would like to acknowledge the use of Servicio General de Apoyo a la Investigación-SAI, Universidad de Zaragoza.

Appendix A. Supplementary data

Supplementary data to this article can be found online at https://doi.org/10.1016/j.biombioe.2025.107778.

Data availability

Data will be made available on request.

References

[1] Key documents: REPowerEU - European commission. https://commission.europa.eu/publications/key-documents-repowereu_en, 2022. (Accessed 19 December 2024).
[2] BOE-A-2022-860 Real Decreto 47/2022, de 18 de enero, sobre protección de las aguas contra la contaminación difusa producida por los nitratos procedentes de fuentes agrarias. https://www.boe.es/buscar/doc.php?id=BOE-A-2022-860, 2022. (Accessed 19 December 2024).
[3] Hoja de Ruta del Biogás, Madrid, https://www.miteco.gob.es/va/energia/novedades/consejo-ministros-aprueba-hoja-ruta-biogas.html, 2022. (Accessed 19 December 2024).
[4] B. Aghel, S. Behaein, F. Alobiad, CO2 capture from biogas by biomass-based adsorbents: a review, Fuel 328 (2022) 125276, https://doi.org/10.1016/J.FUEL.2022.125276.
[5] E. Mulu, M.M. M'Arimi, R.C. Ramkat, A review of recent developments in application of low cost natural materials in purification and upgrade of biogas, Renew. Sustain. Energy Rev. 145 (2021) 111081, https://doi.org/10.1016/J.RSER.2021.111081.
[6] C. Pevida, F. Rubiera, Adsorption processes for CO2 capture from biogas streams, Energies 16 (2023) 667, https://doi.org/10.3390/EN16020667.
[7] C. Goel, S. Mohan, P. Dinesha, CO2 capture by adsorption on biomass-derived activated char: a review, Sci. Total Environ. 798 (2021) 149296, https://doi.org/10.1016/J.SCITOTENV.2021.149296.
[8] S. Guo, Y. Li, Y. Wang, L. Wang, Y. Sun, L. Liu, Recent advances in biochar-based adsorbents for CO2 capture, Carbon Capture Sci. Technol. 4 (2022) 100059, https://doi.org/10.1016/J.CCST.2022.100059.
[9] P.D. Dissanayake, S. You, A.D. Igalavithana, Y. Xia, A. Bhatnagar, S. Gupta, H. W. Kua, S. Kim, J.H. Kwon, D.C.W. Tsang, Y.S. Ok, Biochar-based adsorbents for carbon dioxide capture: a critical review, Renew. Sustain. Energy Rev. 119 (2020) 109582, https://doi.org/10.1016/j.rser.2019.109582.
[10] W. Suliman, J.B. Harsh, N.I. Abu-Lail, A.M. Fortuna, I. Dallmeyer, M. Garcia-Perez, Influence of feedstock source and pyrolysis temperature on biochar bulk and surface properties, Biomass Bioenergy 84 (2016) 37–48, https://doi.org/10.1016/J.BIOMBIOE.2015.11.010.
[11] V. Moset, D. Fontaine, H.B. Møller, Co-digestion of cattle manure and grass harvested with different technologies. Effect on methane yield, digestate composition and energy balance, Energy 141 (2017) 451–460, https://doi.org/10.1016/J.ENERGY.2017.08.068.
[12] R. Kadam, S. Jo, J. Lee, K. Khanthong, H. Jang, J. Park, A review on the anaerobic Co-digestion of livestock manures in the context of sustainable waste management, Energies 17 (2024) 546, https://doi.org/10.3390/EN17030546, 2024, Vol. 17, Page 546.
[13] C. Teater, Z. Yue, J. MacLellan, Y. Liu, W. Liao, Assessing solid digestate from anaerobic digestion as feedstock for ethanol production, Bioresour. Technol. 102 (2011) 1856–1862, https://doi.org/10.1016/J.BIORTECH.2010.09.099.
[14] F. Häfner, J. Hartung, K. Möller, Digestate composition affecting N fertiliser value and C mineralisation, Waste Biomass Valoriza. 13 (2022) 3445–3462, https://doi.org/10.1007/S12649-022-01723-Y.
[15] C. Romio, A.J. Ward, H.B. Møller, Characterization and valorization of biogas digestate and derived organic fertilizer products from separation processes, Front. Sustain. Food Syst. 8 (2024) 1415508, https://doi.org/10.3389/FSUFS.2024.1415508.
[16] Z. Cao, D. Jung, M.P. Olszewski, P.J. Arauzo, A. Kruse, Hydrothermal carbonization of biogas digestate: effect of digestate origin and process conditions, Waste Manag. 100 (2019) 138–150, https://doi.org/10.1016/J.WASMAN.2019.09.009.
[17] E.M. Ekstrand, A. Björn, A. Karlsson, A. Schnürer, L. Kanders, S.S. Yekta, M. Karlsson, J. Moestedt, Identifying targets for increased biogas production through chemical and organic matter characterization of digestate from full-scale biogas plants: what remains and why? Biotechnol. Biofuels Bioprodu. 15 (2022) 1–22, https://doi.org/10.1186/S13068-022-02103-3.
[18] S. Wang, X. Guo, T. Liang, Y. Zhou, Z. Luo, Mechanism research on cellulose pyrolysis by Py-GC/MS and subsequent density functional theory studies, Bioresour. Technol. 104 (2012) 722–728, https://doi.org/10.1016/J.BIORTECH.2011.10.078.
[19] J. Hao, F. Xu, D. Yang, B. Wang, Y. Qiao, Y. Tian, Analytical pyrolysis of biomass using pyrolysis-gas chromatography/mass spectrometry, Renew. Sustain. Energy Rev. 208 (2025) 115090, https://doi.org/10.1016/J.RSER.2024.115090.

[20] L. Zhang, J. Liu, Z. Zhang, Z. Yang, X. Wang, D. Li, R. Lin, Research of the two-step pyrolysis of lignocellulosic biomass based on the cross-coupling of components by Py-GC/MS, Biomass Convers. Biorefin. 13 (2021) 11789–11802, https://doi.org/10.1007/S13399-021-01993-X.
[21] F.X. Collard, J. Blin, A review on pyrolysis of biomass constituents: mechanisms and composition of the products obtained from the conversion of cellulose, hemicelluloses and lignin, Renew. Sustain. Energy Rev. 38 (2014) 594–608, https://doi.org/10.1016/J.RSER.2014.06.013.
[22] P. Biller, A.B. Ross, Pyrolysis GC–MS as a novel analysis technique to determine the biochemical composition of microalgae, Algal Res. 6 (2014) 91–97, https://doi.org/10.1016/J.ALGAL.2014.09.009.
[23] K. Kebelmann, A. Hornung, U. Karsten, G. Griffiths, Intermediate pyrolysis and product identification by TGA and Py-GC/MS of green microalgae and their extracted protein and lipid components, Biomass Bioenergy 49 (2013) 38–48, https://doi.org/10.1016/J.BIOMBIOE.2012.12.006.
[24] J. Li, Y. Li, Y. Wu, M. Zheng, A comparison of biochars from lignin, cellulose and wood as the sorbent to an aromatic pollutant, J. Hazard Mater. 280 (2014) 450–457, https://doi.org/10.1016/J.JHAZMAT.2014.08.033.
[25] R.K. Sharma, J.B. Wooten, V.L. Baliga, X. Lin, W.G. Chan, M.R. Hajaligol, Characterization of chars from pyrolysis of lignin, Fuel 83 (2004) 1469–1482, https://doi.org/10.1016/J.FUEL.2003.11.015.
[26] C. Zhang, Y. Shao, L. Zhang, S. Zhang, R.J.M. Westerhof, Q. Liu, P. Jia, Q. Li, Y. Wang, X. Hu, Impacts of temperature on evolution of char structure during pyrolysis of lignin, Sci. Total Environ. 699 (2020) 134381, https://doi.org/10.1016/J.SCITOTENV.2019.134381.
[27] B. Hao, H. Yang, Z. Han, L. Jin, Y. Li, H. Hu, Correlation between pores and chemical structures for lignin pyrolysis char, Fuel 376 (2024) 132700, https://doi.org/10.1016/J.FUEL.2024.132700.
[28] W. Wang, R. Lemaire, A. Bensakhria, D. Luart, Review on the catalytic effects of alkali and alkaline earth metals (AAEMs) including sodium, potassium, calcium and magnesium on the pyrolysis of lignocellulosic biomass and on the co-pyrolysis of coal with biomass, J. Anal. Appl. Pyrolysis 163 (2022) 105479, https://doi.org/10.1016/J.JAAP.2022.105479.
[29] S. Wang, X. Guo, K. Wang, Z. Luo, Influence of the interaction of components on the pyrolysis behavior of biomass, J. Anal. Appl. Pyrolysis 91 (2011) 183–189, https://doi.org/10.1016/J.JAAP.2011.02.006.
[30] X. Li, K. Cen, J. Li, C. Wang, D. Jia, D. Chen, Effects of co-pyrolysis interaction performance of cellulose and lignin on the gas products and hydrogen generation path, Ind. Crops Prod. 222 (2024) 119858, https://doi.org/10.1016/J.INDCROP.2024.119858.
[31] N. Gil-Lalaguna, Á. Navarro-Gil, H.H. Carstensen, J. Ruiz, I. Fonts, J. Ceamanos, M. B. Murillo, G. Gea, CO2 adsorption on pyrolysis char from protein-containing livestock waste: how do proteins affect? Sci. Total Environ. 846 (2022) 157395 https://doi.org/10.1016/J.SCITOTENV.2022.157395.
[32] S. Rajkovich, A. Enders, K. Hanley, C. Hyland, A.R. Zimmerman, J. Lehmann, Corn growth and nitrogen nutrition after additions of biochars with varying properties to a temperate soil, Biol. Fertil. Soils 48 (2012) 271–284, https://doi.org/10.1007/S00374-011-0624-7.
[33] H. Yang, R. Yan, H. Chen, D.H. Lee, C. Zheng, Characteristics of hemicellulose, cellulose and lignin pyrolysis, Fuel 86 (2007) 1781–1788, https://doi.org/10.1016/J.FUEL.2006.12.013.
[34] M.R. Barr, R. Volpe, R. Kandiyoti, Identifying synergistic effects between biomass components during pyrolysis and pointers concerning experiment design, ACS Sustain. Chem. Eng. 9 (2021) 5603–5612, https://doi.org/10.1021/acssuschemeng.1c00051.
[35] M. Nik-Azar, M.R. Hajaligol, M. Sohrabi, B. Dabir, Mineral matter effects in rapid pyrolysis of beech wood, Fuel Process. Technol. 51 (1997) 7–17, https://doi.org/10.1016/S0378-3820(96)01074-0.
[36] X.G. Li, Y. Lv, B.G. Ma, W.Q. Wang, S.W. Jian, Decomposition kinetic characteristics of calcium carbonate containing organic acids by TGA, Arab. J. Chem. 10 (2017) S2534–S2538, https://doi.org/10.1016/J.ARABJC.2013.09.026.
[37] V. Mamleev, S. Bourbigot, M. Le Bras, J. Yvon, The facts and hypotheses relating to the phenomenological model of cellulose pyrolysis: interdependence of the steps, J. Anal. Appl. Pyrolysis 84 (2009) 1–17, https://doi.org/10.1016/J.JAAP.2008.10.014.
[38] M. Keiluweit, P.S. Nico, M. Johnson, M. Kleber, Dynamic molecular structure of plant biomass-derived black carbon (biochar), Environ. Sci. Technol. 44 (2010) 1247–1253, https://doi.org/10.1021/es9031419.
[39] L. Leng, S. Xu, R. Liu, T. Yu, X. Zhuo, S. Leng, Q. Xiong, H. Huang, Nitrogen containing functional groups of biochar: an overview, Bioresour. Technol. 298 (2020) 122286, https://doi.org/10.1016/J.BIORTECH.2019.122286.
[40] M. Li, Q. Liu, Z. Lou, Y. Wang, Y. Zhang, G. Qian, Method to characterize acid-base behavior of biochar: site modeling and theoretical simulation, ACS Sustain. Chem. Eng. 2 (2014) 2501–2509, https://doi.org/10.1021/sc500432d.
[41] S. Matsuoka, H. Kawamoto, S. Saka, What is active cellulose in pyrolysis? An approach based on reactivity of cellulose reducing end, J. Anal. Appl. Pyrolysis 106 (2014) 138–146, https://doi.org/10.1016/J.JAAP.2014.01.011.
[42] F. Léo, N. Gil-Lalaguna, Z. Afailal, R. Andrade, E. Lora, I. Fonts, Evaluating the Role of Gasification Stages on Evolution of Fuel-N to Deepen in Sustainable Production of NH3, 2023, pp. 371–398, https://doi.org/10.1007/978-981-99-4580-1_12.
[43] O.L. Li, K. Prabakar, A. Kaneko, H. Park, T. Ishizaki, Exploration of Lewis basicity and oxygen reduction reaction activity in plasma-tailored nitrogen-doped carbon electrocatalysts, Catal. Today 337 (2019) 102–109, https://doi.org/10.1016/J.CATTOD.2019.02.058.
[44] N.M. Amer, P. Lahijani, M. Mohammadi, A.R. Mohamed, Modification of biomass-derived biochar: a practical approach towards development of sustainable CO2 adsorbent, Biomass Conver. Biorefin. 1 (2022) (2022) 1–48, https://doi.org/10.1007/S13399-022-02905-3.
[45] S.E. Ban, E.J. Lee, J. Yoon, D.J. Lim, I.S. Kim, J.W. Lee, Role of cellulose and lignin on biochar characteristics and removal of diazinon from biochar with a controlled chemical composition, Ind. Crops Prod. 200 (2023) 116913, https://doi.org/10.1016/J.INDCROP.2023.116913.
[46] H. Marsh, F. Rodríguez-Reinoso, Activated Carbon, Activated Carbon, 2006, pp. 1–536, https://doi.org/10.1016/B978-0-08-044463-5.X5013-4.
[47] S. Kwon, J.J. Pignatello, Effect of natural organic substances on the surface and adsorptive properties of environmental black carbon (char): pseudo pore blockage by model lipid components and its implications for N2-probed surface properties of natural sorbents, Environ. Sci. Technol. 39 (2005) 7932–7939, https://doi.org/10.1021/es050976h.
[48] X. Xu, Y. Kan, L. Zhao, X. Cao, Chemical transformation of CO2 during its capture by waste biomass derived biochars, Environ. Pollut. 213 (2016) 533–540, https://doi.org/10.1016/J.ENVPOL.2016.03.013.
[49] X. Xiong, I.K.M. Yu, L. Cao, D.C.W. Tsang, S. Zhang, Y.S. Ok, A review of biochar-based catalysts for chemical synthesis, biofuel production, and pollution control, Bioresour. Technol. 246 (2017) 254–270, https://doi.org/10.1016/J.BIORTECH.2017.06.163.
[50] X. Zhang, S. Zhang, H. Yang, Y. Feng, Y. Chen, X. Wang, H. Chen, Nitrogen enriched biochar modified by high temperature CO2–ammonia treatment: characterization and adsorption of CO2, Chem. Eng. J. 257 (2014) 20–27, https://doi.org/10.1016/J.CEJ.2014.07.024.
[51] J.J. Manyà, B. González, M. Azuara, G. Arner, Ultra-microporous adsorbents prepared from vine shoots-derived biochar with high CO2 uptake and CO2/N2 selectivity, Chem. Eng. J. 345 (2018) 631–639, https://doi.org/10.1016/J.CEJ.2018.01.092.
[52] X. Zhang, J. Wu, H. Yang, J. Shao, X. Wang, Y. Chen, S. Zhang, H. Chen, Preparation of nitrogen-doped microporous modified biochar by high temperature CO2-NH3 treatment for CO2 adsorption: effects of temperature, RSC Adv. 6 (2016) 98157–98166, https://doi.org/10.1039/c6ra23748g.
[53] M.J. Prauchner, F. Rodríguez-Reinoso, Chemical versus physical activation of coconut shell: a comparative study, Microporous Mesoporous Mater. 152 (2012) 163–171, https://doi.org/10.1016/J.MICROMESO.2011.11.040.
[54] V. Presser, J. McDonough, S.H. Yeon, Y. Gogotsi, Effect of pore size on carbon dioxide sorption by carbide derived carbon, Energy Environ. Sci. 4 (2011) 3059–3066, https://doi.org/10.1039/C1EE01176F.
[55] T. Jalalabadi, M. Drewery, P. Tremain, J. Wilkinson, B. Moghtaderi, J. Allen, The impact of carbonate salts on char formation and gas evolution during the slow pyrolysis of biomass, cellulose, and lignin, Sustain. Energy Fuels 4 (2020) 5987–6003, https://doi.org/10.1039/D0SE01031F.